J|A|C|S
ARTICLES
Published on Web 07/28/2004

Layer-by-Layer Assembled Multilayer Films of Titanate Nanotubes, Ag- or Au-Loaded Nanotubes, and Nanotubes/Nanosheets with Polycations

Renzhi Ma,* Takayoshi Sasaki, and Yoshio Bando

Contribution from the Advanced Materials Laboratory, National Institute for Materials Science (NIMS), Namiki 1-1, Tsukuba, Ibaraki 305-0044, Japan

Received March 1, 2004; E-mail: ma.renzhi@nims.go.jp

Abstract: Aqueous suspensions of hydrothermally synthesized titanate nanotubes and poly(diallyldimethylammonium chloride) (PDDA) have been employed to fabricate multilayer films on various substrates in a layer-by-layer fashion. Atomic force microscopy displays the dense coverage of the substrate surface by the nanotubes. UV−vis absorption spectroscopy confirms the consecutive growth of PDDA/nanotube layer pairs. Single crystalline Ag and Au nanoparticles with narrow size distribution spatially correlating with the nanotubes have been obtained by treating the nanotubes with $AgNO_3$ or $HAuCl_4$ aqueous solution followed by chemical reduction. The noble metal nanoparticles show a strong surface plasmon absorption band. A multilayer film construction of the noble-metal-loaded nanotubes has also been achieved. This process has been further extended to the heteroassembly of nanotubes/nanosheets in different layer sequences.

Introduction

Thin films of titanium oxide (TiO_2) offer great promise for optical, electrical, and photochemical applications including ultraviolet (UV) light shielding, solar energy conversion, photocatalytic ability to break down toxic pollutants, n-type semiconductor, and dielectric layers.[1] Titanium oxide nanoparticles have attracted tremendous interest due to their intriguing physicochemical, nonlinear optical properties and high surface area, which may greatly increase their activity as catalysts or sensitivity as sensors.[2,3] Langmuir−Blodgett (LB) and layer-by-layer (LBL) assembly techniques have been proved a well-established approach to build composite or function-specific multilayer assemblies, e.g., multilayer thin films on planar substrates and, recently, creative designs of nanotube or cage structures with various compositions using different templates such as carbon nanotubes, membrane, or colloidal particles.[4−9] The LBL technique has already been applied to prepare multilayer films of titanium oxide nanoparticles.[10−12] Recently, colloidal titanium oxide ($Ti_{0.91}O_2$) nanosheets were fabricated by completely delaminating a lepidocrocite-type layered protonic titanate $H_xTi_{2-x/4}\square_{x/4}O_4$ ($x \approx 0.7$, $\square$: vacancy) with tetrabutylammonium (TBA^+) ions.[13] The nanosheets exhibit some significant optical properties, e.g., a very sharp optical absorption peak at 265 nm appreciably blue-shifted relative to the absorption onset of bulk titanium oxide.[14] As lepidocrocite-type titanate is inherently negatively charged due to vacancies at Ti positions, successful LBL assembly of unilamellar $Ti_{0.91}O_2$ nanosheets with positively charged polyelectrolytes such as poly(diallyldimethylammonium chloride) (PDDA) as counterions into multilayer films has been demonstrated.[15,16] This process has also been extended to prepare heterocomposite multilayer films of nanoparticles/nanosheets.[17]

On the other hand, template and hydrothermal synthetic routes have led to titanium oxide nanotubes.[18−22] The potential applications of the nanotubes as highly efficient photocatalysis and photovoltaic cells has been investigated.[21−23] Very recently, oriented arrays of titanium oxide nanotubes were successfully fabricated on a Ti foil seeded with TiO_2 nanoparticles in a hydrothermal procedure.[24] In previous reports, different structure

(1) Hangfeldt, A.; Grätzel, M. *Chem. Rev.* **1995**, *95*, 49.
(2) Serpone, N.; Lawless, D.; Khairutdinov, R. *J. Phys. Chem.* **1995**, *99*, 16646.
(3) Beecroft, L. L.; Ober, C. K. *Adv. Mater.* **1995**, 7, 1009.
(4) Decher, G. *Science* **1997**, 277, 1232.
(5) Decher, G. Schlenoff, J. B. *Multilayer thin films: Sequential assembly of nanocomposite materials*; Wiley-VCH: Weinheim, 2003.
(6) Mayya, K. S.; Gittins, D. I.; Dibaj, A. M.; Caruso, F. *Nano Lett.* **2001**, 1, 727.
(7) Sano, M.; Kamino, A.; Okamura, J.; Shinakai, S. *Nano Lett.* **2002**, *2*, 531−533.
(8) Guo, Y. G.; Wang, L. J.; Bai, C. L. *J. Phys. Chem. B* **2003**, *107*, 5441.
(9) Liang, Z. J.; Susha, A. S.; Yu, A. M.; Caruso, F. *Adv. Mater.* **2003**, *15*, 1849.
(10) Kotov, N. A.; Dékány, I.; Fendler, J. H. *J. Phys. Chem.* **1995**, *99*, 13065.
(11) Liu, Y.; Wang A.; Claus, R. *J. Phys. Chem. B* **1997**, *101*, 1385.
(12) Cassagneau, T.; Fendler, J. H.; Mallouk, T. E. *Langmuir* **2000**, *16*, 241.
(13) Sasaki, T.; Watanabe, M. *J. Am. Chem. Soc.* **1998**, *120*, 4682.
(14) Sasaki, T.; Watanabe, M. *J. Phys. Chem. B* **1997**, *101*, 10159.
(15) Sasaki, T.; Ebina, Y.; Watanabe, M.; Decher, G. *Chem. Commun.* **2000**, 2163.
(16) Sasaki, T.; Ebina, Y.; Tanaka, T.; Harada, M.; Watanabe, M. *Chem. Mater.* **2001**, *13*, 4661.
(17) Wang, Z. S.; Sasaki, T.; Muramatsu, M.; Ebina, Y.; Tanaka, T.; Wang, L. Z.; Watanabe, M. *Chem. Mater.* **2003**, *15*, 807.
(18) Hoyer, P. *Langmuir* **1996**, *12*, 1411.
(19) Kasuga, T.; Hiramatsu, M.; Hoson, A.; Sekino, T.; Niihara, K. *Langmuir* **1998**, *14*, 3160.
(20) Kasuga, T.; Hiramatsu, M.; Hoson, A.; Sekino, T.; Niihara, K. *Adv. Mater.* **1999**, *11*, 1307.
(21) Adachi, M.; Murata, Y.; Yoshikawa, S. *Chem. Lett.* **2000**, *8*, 942.
(22) Uchida, S.; Chiba, R.; Tomiha, M.; Masaki, N.; Shirai, M. *Electrochemistry* **2002**, *70*, 418.
(23) Li, D.; Xia, Y. N. *Nano Lett.* **2003**, *3*, 555.
(24) Tian, Z. R.; Voigt, J. A.; Liu, J.; Mckenzie, B.; Xu, H. *J. Am. Chem. Soc.* **2003**, *125*, 12384.

10.1021/ja048855p CCC: $27.50

models such as anatase and trititanate ($H_2Ti_3O_7$) were proposed for the hydrothermally synthesized nanotubes.[19,24−26] Our recent results indicated that the nanotubes might be of lepidocrocite-type protonic titanate nature.[27] Consequently, the outer surfaces may be negatively charged due to Ti vacancies, the same as nanotubes directly scrolled up from $Ti_{0.91}O_2$ unilamellar nanosheets.[28] It is thus plausible to look into the regular film growth via sequential adsorption of titanate nanotubes with oppositely charged polyelectrolytes. The LBL assembly technique has been applied to build up thin films of chemically solubilized single-wall carbon nanotubes.[29−31] We thus expect it will be possible to achieve the LBL assembly of titanate nanotubes into multilayer structures.

Metal nanoparticles highly dispersed on an active oxide are a classic example of high-performance and heterogeneous catalysts. Efforts have been made on catalytic nanoarchitecture design, e.g., mesoporous or aerogel hosts (silica, TiO_2) impregnated with gold (Au), silver (Ag), platinum (Pt), or other metals, allowing much enhanced access of guest molecules to catalytic centers.[32,33] The typical mesoporous oxides are usually an order of magnitude or more larger than their metallic partner. Titanate nanotubes yield high specific surface area with a nanoscale inner core cavity and exposed outer surface, offering a unique reaction vessel for nanoscale photoactive building blocks. It is therefore of great interest to encapsulate or adorn the titanate nanotubes with noble nanoparticles such as Ag and Au. The diameter (∼10 nm) of the titanate nanotubes is comparable to the desirable size limit, a few nanometers, of noble metal nanoparticles. The specific template effect of the nanotubes may also effectively prevent or minimize the agglomeration of the nanoparticles. This architecture design should, therefore, be ideal for the metal nanoparticles to exhibit high reactivity and enhanced catalytic efficiency, surface plasmon absorption, or nonlinear optical properties. Furthermore, through this new concept of integrating noble metallic particles with a negatively charged crystalline oxide nanotube host, it may be feasible and convenient to fabricate multilayer films of nanotubes with metal loading for potential optoelectrical, photocatalytical, and photovoltaic applications.

We report herein the successful fabrication of metal-oxide composite nanostructures with the integration of Ag and Au nanoparticles with titanate nanotubes. After obtaining a stable aqueous suspension of the nanotubes, we obtained the LBL assembly of titanate nanotube multilayer films with or without the noble metal loading. As an example of heteroassembly, we design the multilayer composite films of nanotubes/nanosheets with optional positioning of individual layers. The UV−vis absorption properties of these multilayer films are characterized. This simple but versatile approach may facilitate the preparation of tailor-made, multicomponent, and multifunction nanofilm devices based on titanate nanotubes.

Experimental Section

Reagents and Materials. Polyethylenimine (PEI), 50 wt % aqueous solution, and poly(diallyldimethylammonium chloride) (PDDA), 20 wt % aqueous solution, were purchased from Aldrich Co. and used without further purification. All other chemicals used were of analytical grade. A Milli-Q water (resistivity > 17 MΩ cm) was used throughout the experiments.

Titanate nanotubes were synthesized by the hydrothermal treatment of anatase-type titanium oxide in concentrated 10 M NaOH solution at 110−150 °C.[27] The obtained nanotubes, 8−12 nm in diameter and several hundred nanometers in length, usually entangle or aggregate together.

Noble metal nanoparticles of Ag and Au in and on the nanotubes were synthesized by reducing $AgNO_3$ and $HAuCl_4$ with $NaBH_4$. In a typical synthesis, titanate nanotubes (50 mg) were dispersed in 100 cm^3 of 0.1 M $AgNO_3$ or $HAuCl_4$ solution in a round-bottom flask. The mixed suspension was magnetically stirred to fill the hollow cylinder of the nanotubes with the $AgNO_3$ or $HAuCl_4$ aqueous solution by capillary suction. The stirring continued for 12 h to promote complete filling. The filled nanotubes were separated from the solution by centrifugation at 6000 rpm. $NaBH_4$ solution (5 cm^3, 0.1 M) was added dropwise to the centrifuged sample. The product, Ag- or Au-loaded nanotubes, was obtained by centrifugation of the reaction mixture.

A colloidal suspension of $Ti_{0.91}O_2$ was synthesized by delaminating $H_{0.7}Ti_{1.825}\square_{0.175}O_4{\cdot}H_2O$ (□: vacancy) with tetrabutylammonium hydroxide (TBAOH) solution.[13] The opalescent suspension contains single layer nanosheets of $Ti_{0.91}O_2$ with a lateral size of 0.1−1 μm.

Fabrication of Self-Assembled Films. A PEI solution (1.25 g dm^{-3}) and the $Ti_{0.91}O_2$ nanosheet suspension (0.08 g dm^{-3}) were added with a dilute HCl solution to adjust their pH to 9, while a PDDA solution (20 g dm^{-3}) containing 0.5 mol dm^{-3} NaCl was added with a TBAOH solution to make its pH 9. Titanate nanotube suspensions (0.05−1.0 g dm^{-3}) were prepared by ultrasonically dispersing the required amount of nanotubes or metal-loaded nanotubes in Milli-Q water for ∼1 h. The pH of the nanotube suspensions was also adjusted to 9 with a dilute TBAOH solution.

Quartz glass slides and silicon wafers were used as substrates after they were cleaned by immersion in a bath of 1:1 methanol/HCl and concentrated H_2SO_4 for 30 min each. Substrates were precoated with a thin PEI layer by dipping them in a PEI solution for 20 min. The substrate surface became positively charged through this procedure. The first layer of nanotubes was prepared by immersing the substrate in the nanotube suspension for 20 min. From the second layer, PDDA was used as a self-assembly counterion. Multilayer films of PDDA and nanotubes, $(PDDA/nanotube)_n$, were prepared by repeating the following steps *n* times: (1) immersing in the PDDA solution for 20 min; (2) washing with Milli-Q water; (3) immersing in nanotube suspension for 20 min; (4) washing with Milli-Q water followed by drying under N_2 gas flow. Heteroassembled composite films of nanotubes/nanosheets were fabricated by alternating sequential adsorption in the suspensions of nanotubes and nanosheets.

Instrumentation. Transmission electron microscopy (TEM) characterizations were performed using a high-resolution transmission electron microscope (HRTEM, JEM-3000F, JEOL) with energy-dispersive X-ray spectrometer (EDS). UV−vis absorption spectra were recorded on a Hitachi U-4000 spectrophotometer. A Seiko SPA 400 atomic force microscopy (AFM) system was used to examine the surface topography of the films prepared on Si wafers. AFM images were acquired in tapping-mode using a Si tip cantilever with a force constant of 20 N cm^{-1}.

(25) Chen, Q.; Du, G. H.; Zhang, S.; Peng, L. M. *Acta Crystallogr., Sect. B* **2002**, *58*, 587.
(26) Yao B. D.; Chan, Y. F.; Zhang, X Y.; Zhang, W. F.; Yang, Z. Y.; Wang N. *Appl. Phys. Lett.* **2003**, *82*, 281.
(27) Ma, R.; Bando, Y.; Sasaki, T. *Chem. Phys. Lett.* **2003**, *380*, 577.
(28) Ma, R.; Bando, Y.; Sasaki, T. *J. Phys. Chem. B* **2004**, *108*, 2115.
(29) Mamedov, A. A.; Kotov, N. A.; Prato, M.; Guldi, D. M.; Wicksted, J. M.; Hirsch, A. *Nat. Mater.* **2002**, *1*, 190−194.
(30) Rouse, J. H.; Lillehei, P. T. *Nano Lett.* **2003**, *3*, 59.
(31) Kim, Y.; Minami, N.; Zhu, W.; Kazaoui, S.; Azumi, R.; Matsumoto, M. *Jpn. J. Appl. Phys.* **2003**, *42*, 7629.
(32) Rolison, D. R. *Science* **2003**, *299*, 1698.
(33) Guari, Y.; Thieuleux, C.; Mehdi, A.; Reye, C.; Corriu, R. J. P.; Gomez-Gallardo, S.; Philippot, K.; Chaudret, B.; Dutartre, R. *Chem. Commun.* **2001**, 1374.

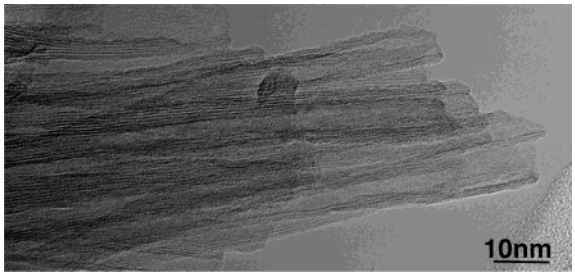

Figure 1. TEM image of hydrothermal synthesized titanate nanotubes.

Results and Discussion

Loading of Metal Nanoparticles in/onto Nanotubes. Figure 1 displays a typical TEM image of the hydrothermally synthesized titanate nanotubes. Besides a uniform diameter distribution (inner, 3−5 nm; outer, 8−12 nm), the nanotubes are always open on both ends, enabling solution filling or nanocluster encapsulation into their tubular cavity.

Figure 2a shows representative TEM images of the nanotubes after the immersion in the $AgNO_3$ aqueous solution and the subsequent reduction with $NaBH_4$. Nanoparticles measuring a few nm in dimension are supported on the nanotubes. High magnification TEM images clearly demonstrate that the nanoparticles are both encapsulated in or coated on the nanotubes (Figure 2b,c). The elongated shape of the encapsulated nanoparticle reflects the confinement and template effect by the one-dimensional nanospace of the nanotubes. TEM statistical analysis reveals that the size of nanoparticles is distributed mostly in a range of 3−10 nm. The selected area electron diffraction (SAED) pattern from several nanoparticles is shown in Figure 2d. The characteristic rings of the polycrystalline diffraction pattern can be indexed to (111), (200), (220), (311), and (331) for *fcc* Ag. A nanobeam diffraction (beam size 0.8 nm) from a single nanoparticle shown in Figure 2e can be ascribed to the [110] projection of the *fcc* Ag. This diffraction feature shows that every individual nanoparticle is a single crystalline nanocrystal. The EDS measurements confirm the metallic Ag composition (Figure 2f). Figure 2f also shows signals of copper, titanium, and oxygen originated from the copper grid and titanate nanotubes.

The typical TEM image from the obtained product after reducing nanotubes in $HAuCl_4$ solution reveals that Au nanocrystals are confined in the hollow cavity or supported on the surface of nanotubes (Figure 3a). Figure 3b depicts an HRTEM image revealing the single crystalline *fcc* Au nanocrystal with a clearly resolved lattice fringe of (111) ($d = 0.24$ nm). Most of the Au nanocrystals have dimensions of 2−6 nm. The EDS in Figure 3c indicates the exact elemental composition of Au. The absence of Cl signals also supports the supposition that the Au ions have been completely reduced to Au crystals.

From the above characterizations, it is obvious that the noble metal ions (Ag^+, Au^+) are readily converted to metallic

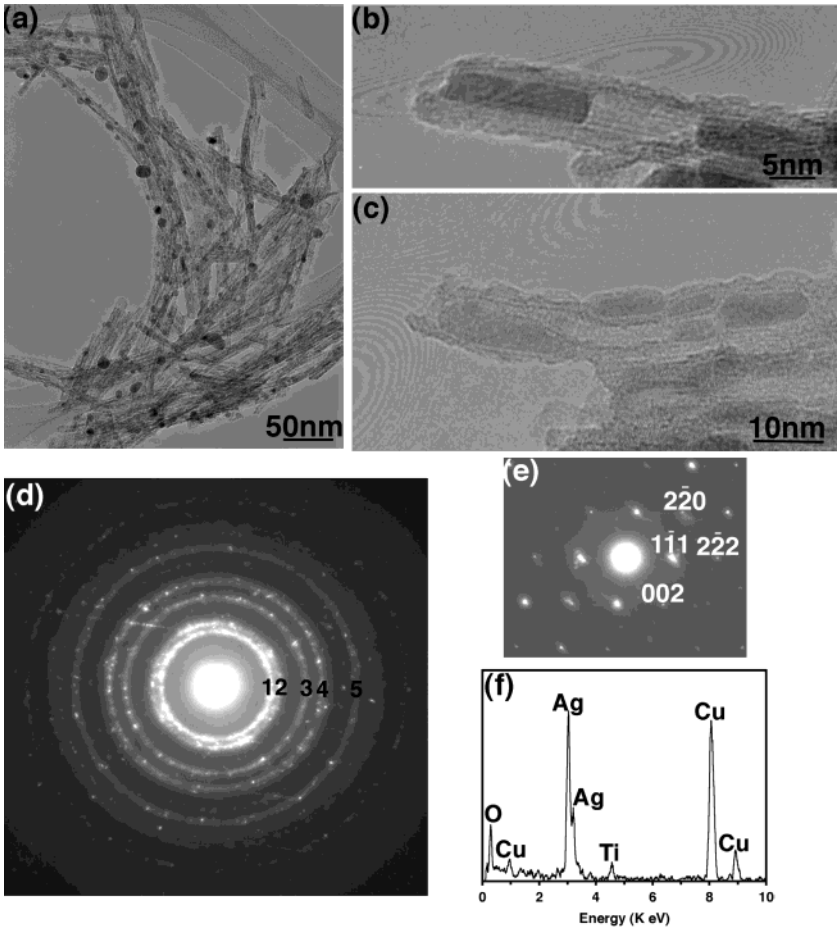

Figure 2. Ag-loaded nanotubes. (a) Typical TEM image depicting the abundant nanoparticles spatially correlating with nanotubes. (b,c) High magnification image showing the nanoparticles are both confined and supported on nanotubes. (d) SAD pattern gives polycrystalline rings numbered 1, 2, 3, 4, and 5 consistent with (111) (0.236 nm), (200)(0.208 nm), (220) (0.147 nm), (311) (0.125 nm), and (331) (0.095 nm) of *fcc* Ag. (e) Nanobeam diffraction pattern demonstrates the single crystalline feature of each Ag nanoparticle. The pattern can be indexed to be the [110] zone axis of *fcc* Ag. (f) EDS of Ag nanocrystals.

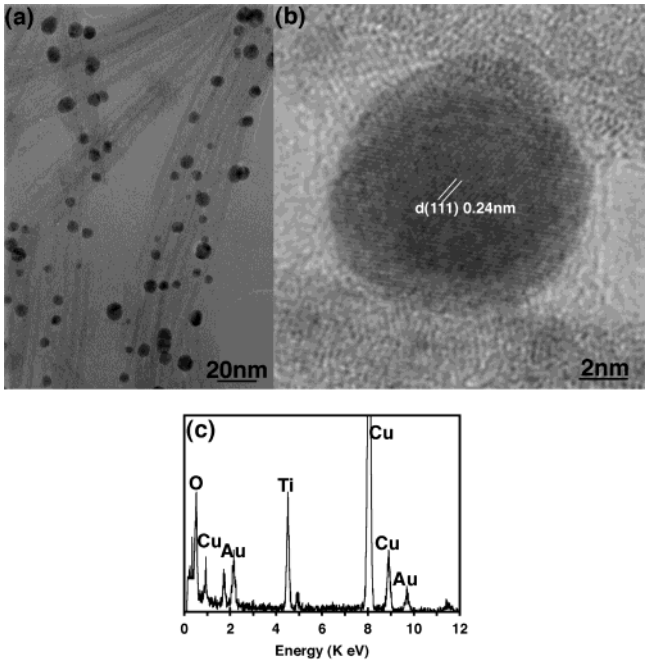

Figure 3. Au-loaded nanotubes. (a) Typical TEM image. (b) HRTEM image showing the clearly resolved lattice image of *fcc* Au ($d(111) = 0.24$ nm). (c) EDS of Au nanocrystals.

nanoparticles by chemical reduction. On the basis of TEM observations, we estimate that ~40% of the nanotubes encapsulate Ag or Au nanoparticles. There are also abundant nanoparticles coated on the nanotube surface. The simple estimation of the nanoparticle locations inside or outside the nanotubes is based on the TEM observation whether they are fully confined in the inner cores or not (For a more exact determination, it is necessary to rotate the sample holder and observe the positioning changes during the rotation to see whether the nanoparticles remain in the inner cores or move away.). The crucial step for the present method is in the drawing of the $AgNO_3$ or $HAuCl_4$ aqueous solution into the hollow cylinder of titanate nanotubes through capillary force. The presence of abundant nanoparticles outside the nanotubes indicates that $AgNO_3$ or $HAuCl_4$ aqueous solution might easily outflow from the nanotubes during the $NaBH_4$ reduction process. Another possibility is that some residual $AgNO_3$ or $HAuCl_4$ solution persists in the interstitial space between adjacent nanotubes. Metal nanoparticles yielded from the outflow or residual precursor solution are adsorbed onto the nanotube surfaces. The ligand-free metallic nanoparticles are stably kept on the nanotube surface. This stability probably arises from strong bonding interaction between the surface atoms of the nanoparticles and the surrounding oxygen atoms of the nanotubes. It is noteworthy that almost all the nanoparticles spatially correlate with the nanotubes. In other words, there are no separated Ag or Au nanoparticles without the confinement or support of nanotubes. The same reaction in the absence of nanotubes produced aggregated metal nanoparticles (20−50 nm). It is very clear that titanate nanotubes serve as effective nanoreactors for in situ chemical transformation of monodispersed metallic nanocrystals without coagulation and bulk growth.

When the nanotubes are ultrasonically dispersed in Milli-Q water, a translucent suspension can be obtained. The suspension remains visually stable without precipitation for months. Instead, bright yellow or purple colors are exhibited, respectively, for

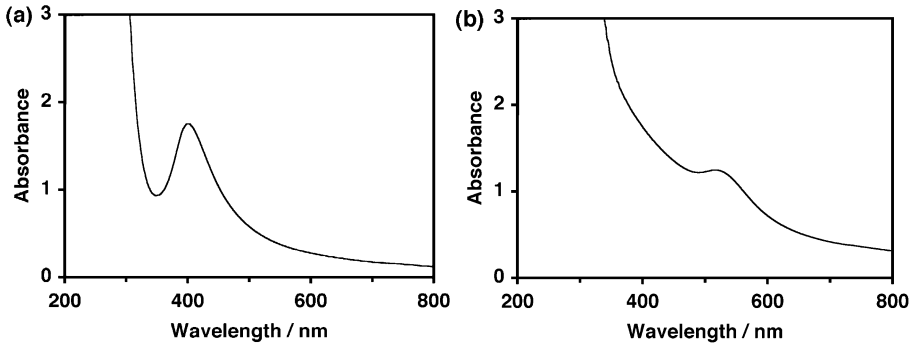

Figure 4. UV−vis absorption spectra of Ag- and Au-loaded titanate nanotube suspensions. (a) The Ag-loaded nanotube suspension (0.2 g dm^{-3}) exhibits a strong absorption band at ~400 nm. (b) The Au-loaded nanotube suspension (0.4 g dm^{-3}) has an absorption band centered at ~520 nm.

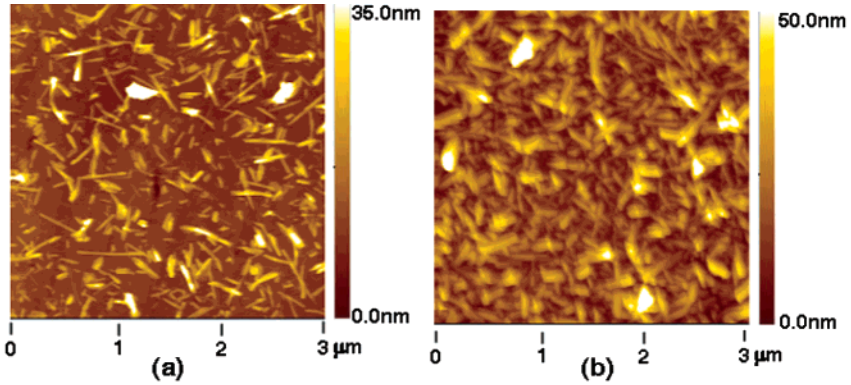

Figure 5. AFM images of the first nanotube layer deposited on a PEI-coated Si wafer from different nanotube concentrations (a) 0.08 g dm^{-3} and (b) 0.36 g dm^{-3}.

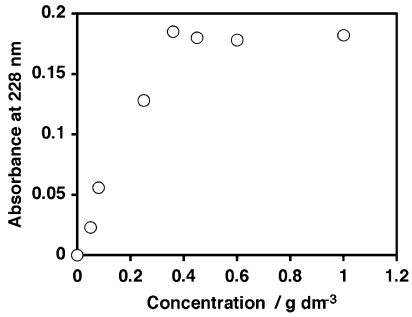

Figure 6. Relationship between absorbance at 228 nm of a PDDA/nanotube layer pair and concentration of nanotube suspension with a fixed deposition time of 20 min.

suspensions of Ag- or Au-loaded nanotubes. The sample colors originate from the surface plasmon absorption of Ag or Au nanoparticles. Noble metal nanoparticles show strong optical absorption in the visible area caused by the collective excitation of the free electron gas. This coherent electron motion gives rise to the surface plasmon absorption.[34−36] The resonance frequency as well as the width of the plasmon absorption band depends on the nanoparticle size and shape. Figure 4 shows the UV−vis absorption spectra collected from the Ag- and Au-loaded nanotube suspensions. The strong absorption between 200−300 nm in both spectra originates from titanate nanotubes, which is characteristic of titanium oxide-based materials. The strong absorption band at ∼400 nm in Figure 4a is attributed to the surface plasmon resonance of metallic Ag nanoparticles. On the other hand, the surface plasmon absorption of gold nanoparticles is characterized by the absorption band in the visible region centered at ∼520 nm (Figure 4b). These absorption bands agree well with the previous reports on metallic Ag and Au spherical nanoparticles with narrow size distribution.[34,35] Some work showed that the aspect ratio (length divided by width) of nanoparticles might affect the absorption spectra. In the regime of high aspect ratio, the peak position might be either red-shifted (e.g., Au nanorods)[35] or blue-shifted (e.g. Ag nanowires).[36] This kind of position shift is not apparent for the present nanoparticles possibly due to their relatively low aspect ratio.

Multilayer Assemblies of Nanotubes and Nanosheets. By immersing in PEI solution, a cationic surface is produced on Si or quartz glass substrates. Figure 5a shows the tapping-mode AFM images of the first deposited layer of titanate nanotubes on a PEI-coated Si wafer fabricated from a nanotube suspension of 0.08 g dm^{-3}. The surface is covered with rod-shaped crystallites although there are also apparent uncovered areas. Section analysis reveals the rod-shaped crystallites have an average thickness of 11 ± 2 nm, in good agreement with the TEM observation on nanotube diameters. This image also reflects the well-dispersed feature of the starting nanotube suspension. The coverage of the surface increases with higher concentration of the nanotube suspension or with prolonged deposition time. The substrate surface appeared to be densely covered with nanotubes when a nanotube concentration of 0.36 g dm^{-3} and a deposition time of 20 min were employed (Figure 5b). As the nanotubes are usually several hundred nanometers in length, the overlapping of some nanotubes may be inevitable. However, the standard vertical distance deviation on different areas was generally ∼8 nm, suggesting that the surface of the nanotube layer was fairly flat.

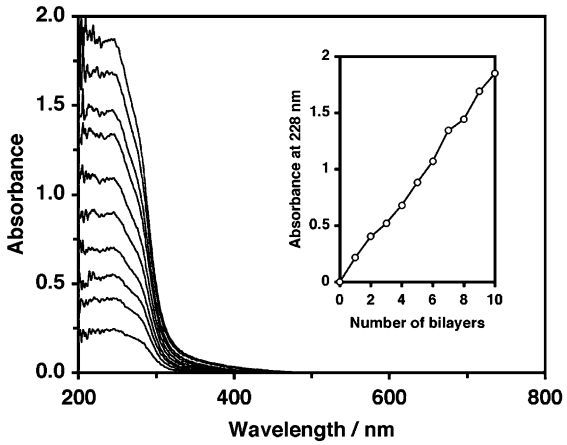

Figure 7. UV−vis absorption spectra for PDDA/nanotube multilayer film fabricated from a nanotube concentration of 0.36 g dm^{-3} and deposition time of 20 min. (Inset) A plot of absorbance at 228 nm vs the number of layer pairs.

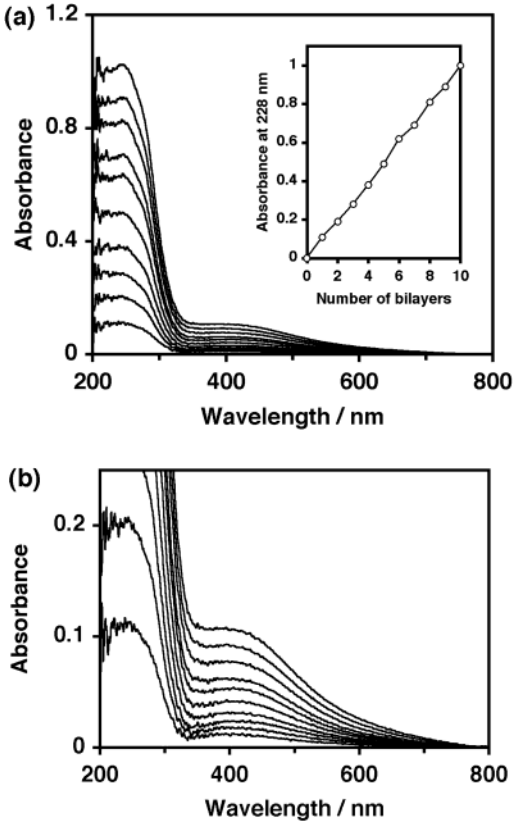

Figure 8. (a) UV−vis absorption spectra for Ag-loaded nanotube multilayer deposited from the nanotube concentration of 0.2 g dm^{-3} and deposition time of 20 min. (Inset) A plot of absorbance at 228 nm vs the number of layer pairs. (b) Enlarged spectra showing the enhanced characteristic absorption band at ∼400 nm originated from Ag nanoparticles.

Consecutive adsorption procedures of PDDA/nanotube layer pairs (each layer on both sides of the substrate) yield visibly transparent thin films. The nanotubes give a broad absorption band between 200 and 300 nm. In referring to titanium oxide nanoparticles,[17] we consider a peak-top value at ∼228 nm as

(34) Henglein, A. *J. Phys. Chem*. **1993**, *97*, 5457.
(35) Mohamed, M. B.; Volkov, V.; Link, S.; El-Sayed, M. A. *Chem. Phys Lett*. **2000**, *317*, 517.
(36) Sun, Y.; Yin, Y.; Mayers, B.; Herricks, T.; Xia, Y. *Chem. Mater*. **2002**, *14*, 4736.

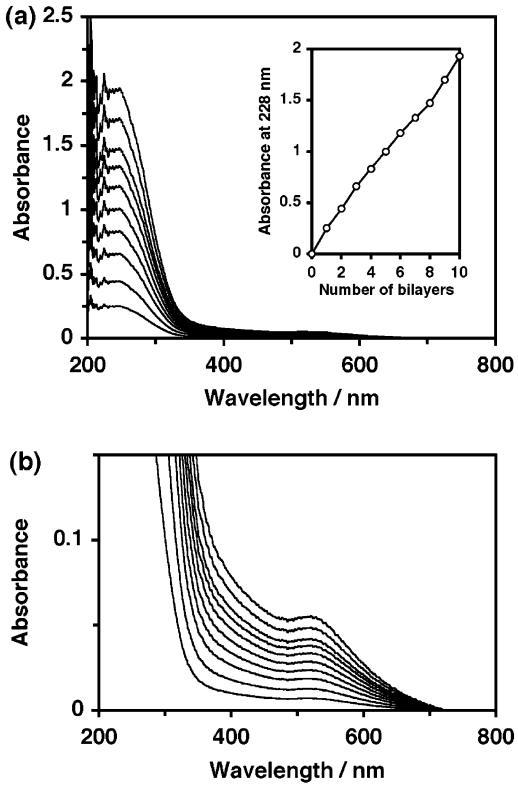

Figure 9. (a) UV−vis absorption spectra for Au-loaded nanotube multilayer deposited from the nanotube concentration of 0.4 g dm^{-3} and deposition time of 20 min. The inset is a plot of absorbance at 228 nm vs the number of layer pairs. (b) The characteristic absorption bands of Au nanoparticles centered at ~520 nm are enhanced with increasing number of layers.

the nominal absorbance of the nanotubes. Figure 6 shows the UV−vis absorbance of the PDDA/nanotube layer pair deposited on a quartz glass slide as a function of the nanotube suspension concentration for a fixed deposition time of 20 min. The absorbance at 228 nm increases until the nanotube suspension concentration reaches 0.36 g dm^{-3}. A plateau occurs at above 0.36 g dm^{-3} or time longer than 20 min, suggesting saturation of nanotube adsorption on the surface.

The regularities of the multilayer deposition are also monitored by recording the UV−vis absorption spectra of the resulting films immediately after each layer pair buildup cycle. The spectra of 1−10 PDDA/nanotube layer pair film from a nanotube suspension of 0.36 g dm^{-3} on a quartz glass slide are shown in Figure 7. It is clearly seen that the absorbance increases almost in proportion to the number of layer pairs. The modest increase in background at a wavelength of >300 nm may arise from light scattering. The inset plot depicts the absorption intensity at 228 nm vs the number of layer pairs. A linear fit yields an average increase of the absorption intensity of 0.185 per layer pair. This linear dependence provides a powerful criterion for the stepwise and regular film growth process. Consequently, an approximately equal amount of nanotubes is deposited for each layer pair adsorption procedure.

LBL assembly also allows the multilayer film construction of Ag- and Au- loaded nanotubes. Figure 8a displays the UV−vis spectra for multilayer films of PDDA/Ag-nanotubes. Besides the linear increase of the nanotube absorbance at 228 nm (inset), there is substantial enhanced absorption at a wavelength >300 nm. The enlarged spectra in Figure 8b clearly demonstrate the characteristic absorption band of Ag nanoparticles at ~400 nm.

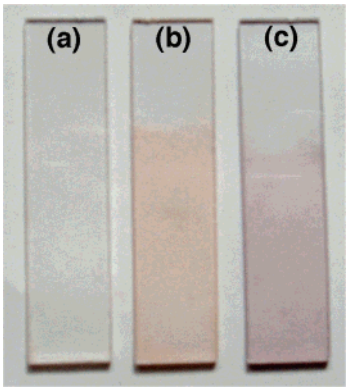

Figure 10. Photographs of multilayer films deposited on quartz glass slides. (a) Quartz/PEI/nanotube/$(PDDA/nanotube)_9$. (b) Quartz/PEI/Ag-nanotube/$(PDDA/Ag\text{-}nanotube)_9$. (c) Quartz/PEI/Au-nanotube/$(PDDA/Au\text{-}nanotube)_9$.

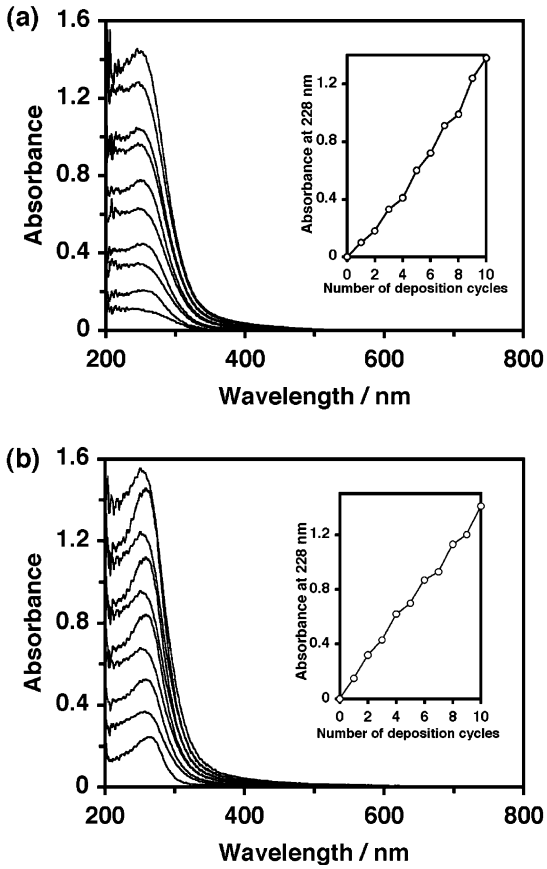

Figure 11. UV−vis absorption spectra for heteroassembled multilayer films of nanotubes/nanosheets in two reversal sequences. (a) Quartz/PEI/nanotube/$(PDDA/nanosheet/PDDA/nanotube)_4$/PDDA/nanosheet. (b) Quartz/PEI/nanosheet/$(PDDA/nanotube/PDDA/nanosheet)_4$/PDDA/nanotube. The insets in both spectra show the increase of absorption at 228 nm with the number of deposition cycles.

The almost regular increment provides strong evidence for the successful fabrication of multilayer films of nanotubes incorporating Ag.

In a similar manner, Figure 9 shows the UV−vis spectra of Au-loaded nanotube films. It is also apparent that the regular film growth of Au-loaded nanotubes has been achieved. A photograph of the resulting 10-layer pair films of Ag- and Au-loaded nanotubes, in comparison with the transparent nanotube film, is shown in Figure 10. The Ag- and Au-loaded films exhibit light yellow and purple coloring, respectively, consistent

with the sample colors of the starting nanotube/nanoparticle suspensions.

Based on the same LBL technique, heterocomposite films comprising nanotube/nanosheet by alternately assembling layer pairs of PDDA/nanotube and PDDA/nanosheet also have been successfully fabricated. The nanotube and nanosheet in the composite films can be layered in any desired order. Figure 11 shows the UV−vis absorption spectra for LBL assembly of nanotubes and nanosheets in two different alternations. The optical features attributable to nanotubes and nanosheets appear as a simple sum of each layer pair component for PDDA/nanotube and PDDA/nanosheet. The average increases in absorption for PDDA/nanotube (at 228 nm) and PDDA/nanosheet (at 265 nm) are comparable to those observed for the multilayer buildup process of each layer pair alone (see inset in Figure 11). This regular enhancement unambiguously indicates the successful intergrowth of nanotubes with nanosheets in the multilayer films.

Recent electrochemical and photoelectrochemical work have revealed the electronic band structure of the two-dimensional nanosheets with a band gap approximately 0.6 eV larger than the values of anatase-type TiO_2.[37] The nanosheets are electronically isolated in the multilayer assemblies. As the one-dimensional tubular morphology of nanotubes is very different from that of anatase-type TiO_2 and two-dimensional nanosheets, some new electrochemical or photoelectrochemcial properties may be expected from the multilayer nanotube, nanotube/metal, or nanotube/nanosheet films. The investigations are under way.

Conclusion

This work demonstrates a general approach for the design and assembly of nanoarchitectures based on titanate nanotubes. Titanate nanotubes provide an opportunity for template synthesis, catalyst support, and heterogeneous catalysis through the incorporation with monodispersed Ag and Au nanoparticles. After attaining the stable suspension of nanotubes, the negative charge characteristic of titanate nanotubes offers a strong tool and dynamic control of the organization and combination of ordered nanofilms. Regular multilayer films of titanate nanotubes, Ag- or Au-loaded nanotubes, and nanotube/nanosheet heterocomposites have been successfully fabricated in a sequential LBL assembly with polycations. This process may be explored for custom synthesis of titanate nanotube-based multicomponent and multifunction ultrathin films for various applications in photocatalysis, solar energy conversion, and electrochromic and self-cleaning devices.

Acknowledgment. The work has been supported by CREST of the Japan Science and Technology Agency (JST). After this manuscript had been submitted for review, we noticed a report published on the multilayer film fabrication of TiO_2 nanotubes by Tokudome et al. (*Chem. Commun*. **2004**, *8*, 958). We acknowledge this important contribution.

Note Added after ASAP Publication: There was a wording error in the first paragraph heading in the Results and Discussion in the version published on the Web July 28, 2004. The final Web version published July 30, 2004 and the print version are correct.

JA048855P

(37) Sakai, N.; Ebina, Y.; Takada, K.; Sasaki, T. *J. Am. Chem. Soc.* **2004**, *126*, 5851.